ELSEVIER

Journal of Organometallic Chemistry 643–644 (2002) 307–312

Journal of Organometallic Chemistry

www.elsevier.com/locate/jorganchem

Synthesis and characterization of monodisperse zinc and zinc oxide nanoparticles from the organometallic precursor $[Zn(C_6H_{11})_2]$

Franck Rataboul [a], Céline Nayral [a], Marie-José Casanove [b], André Maisonnat [a,*], Bruno Chaudret [a,*]

[a] *Laboratoire de Chimie de Coordination du CNRS, UPR 8241, 205 route de Narbonne, F-31077 Toulouse, Cedex 04, France*

[b] *Centre d'Elaboration des Matériaux et d'Etudes structurales du CNRS, UPR 8011, 29, rue Jeanne Marvig BP 4347, F-31055 Toulouse, Cedex 04, France*

Received 13 July 2001; accepted 9 October 2001

Dedicated to François Mathey on his 60th birthday in recognition of his pioneering work in main group and organometallic chemistry

Abstract

Decomposition of the organometallic precursor $[Zn(C_6H_{11})_2]$ in wet anisole leads to the formation of monodisperse spherical Zn particles of 6 nm mean diameter. High resolution electron microscopy (HRTEM) indicates the crystalline nature of these particles and photoelectron studies (XPS) are consistent with the presence of both zinc and zinc oxide. In the presence of polyvinylpyrolidone (PVP), the decomposition leads to well dispersed nanoparticles for which HRTEM studies evidenced the presence of hexagonal zinc (0) surrounded by a thin layer of hexagonal zinc oxide of wurtzite type. The thermal oxidation of these zinc nanoparticles yields well-crystallized nanoparticles of ZnO without coalescence or size change. An X-ray diffraction pattern shows that the powder consists of pure hexagonal wurtzite-type phase.

Keywords: Zinc; Zinc oxide; Nanoparticles; Organometallic precursor

1. Introduction

The precise control of the morphology of semi-conducting oxide materials at the nanometric scale is of basic importance for a fine-tuning of their physical properties such as electrical conductivity or magnetic, optical and mechanical characteristics, and for the wide range of applications in which these properties are implemented, e.g. gas sensors, varistors, transducers, photocells, UV absorbing materials or pigment additives.

For example, the optical properties of nano-sized luminescent semi-conducting particles are known to be substantially different from those of bulk materials [1–3]. The electrical properties of polycrystalline metal-oxide materials depend strongly on their morphology, and it has been reported that the nominal voltage of ZnO-based varistors decreases linearly as the average size of the ZnO grains decreases [4]. Similarly, the sensitivity of SnO_2-based gas sensors is expected to increase as the average size of the individual grains decreases [5–7].

Concerning zinc oxide itself, its industrial applications are of particular importance and the gas sensing properties [8–11] as well as the optical properties [1,2,12,13] and varistor applications [14–17] are subjects of extensive studies. In these applications, the sol–gel route yielding zinc oxide colloids is widely used. This leads generally to polycrystalline materials that require subsequent thermal treatments in order to improve their stability and the reproducibility of their properties. However, thermal treatments lead to structural modifications (increase of the mean grain size, spreading of the grain size distribution, etc.) with increasing annealing temperature. Synthesis of zinc particles in a first step followed by their oxidation can be viewed as an alternative process to prepare ZnO particles displaying a low size dispersion. There are, however, few reports dealing with the synthesis of

* Corresponding authors. Tel.: +33-561-333179; fax: +33-561-553003 (A.M.); Tel.: +33-561-333181; fax: +33-561-553003 (B.C.).

E-mail addresses: maisonat@lcc-toulouse.fr (A. Maisonnat), chaudret@lcc-toulouse.fr (B. Chaudret).

0022-328X/02/$ - see front matter
PII: S0022-328X(01)01378-X

zerovalent zinc particles. The most common methods involve physical processes such as thermal evaporation of bulk zinc and condensation of vapors in an inert gas atmosphere [11,18–21] or co-condensation with organic solvent vapors [22,23]. This includes also the photochemical decomposition of dimethyl zinc in a PVD process [24]. Alternative chemical methods like homogeneous reduction of metal salts producing metal colloids in non-aqueous solvents have also been reported [25].

We have previously shown that the synthesis of metal nanoparticles of controlled size, composition and surface state could be achieved by decomposition of organometallic precursors in mild conditions by thermal activation or by a chemical process involving the presence of a reactive gas. This method has been successfully applied to the preparation of monodisperse nanoparticles of noble and magnetic metals [26–30]. It has been extended to the preparation of alloys [31] and of monodisperse tin and indium nanoparticles. Tin nanoparticles, easily oxidize into well-crystallized tin dioxide nanoparticles without change in the size, and constitute a convenient starting material to generate sensitive semiconducting layers in miniaturized gas sensors [32–34]. Indium nanoparticles can be spontaneously organized in super lattices in the presence of trioctylphosphine oxide [35].

In this paper, we demonstrate that the organometallic approach can be extended to the case of zinc and we describe hereafter the synthesis of well crystallized zinc and zinc oxide nanoparticles together with their characterization by electron microscopy, photoelectron spectroscopy and X-ray diffraction studies.

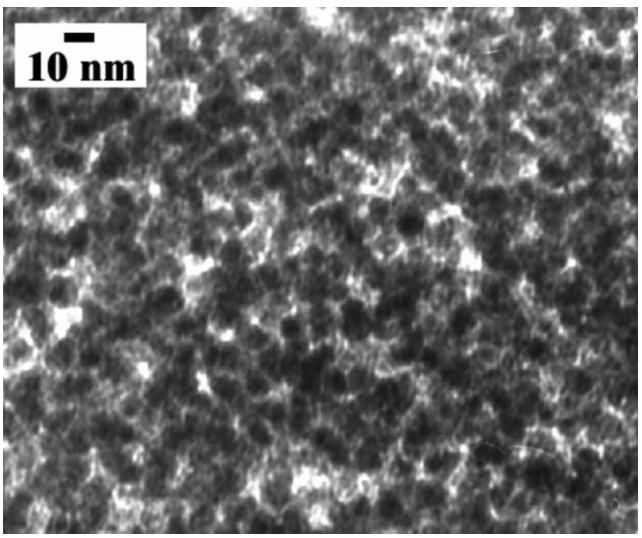

Fig. 1. TEM image of Zn nanoparticles prepared by thermolysis of $ZnCy_2$ in anisole at 130 °C.

2. Results and discussion

Homoleptic amido zinc complexes as well as organozincic complexes are potential precursors for the synthesis of metal nanoparticles, owing to thermochemical data which suggest the low thermodynamic stability of the Zn–N and Zn–C bonds. In fact, in contrast with tin amido complexes from which tin–tin oxide nanoparticles were easily obtained upon thermal activation, the homoleptic amido zinc complexes $\{Zn[N(SiMe_3)_2]_2\}$ and $\{Zn[N^iPr_2]_2\}$ do not lead to decomposition products. However, interesting results were obtained starting from the bis(cyclohexyl) zinc complex. $[Zn(C_6H_{11})_2]$ was prepared according to published method starting from $ZnCl_2$ and $(C_6H_{11})MgCl$ [36]. Crystals of $[Zn(C_6H_{11})_2]$ decompose in a single step near 180 °C under flowing helium in a thermogravimetric equipment with a weight loss of 72% consistent with the formation of pure metal residues.

In toluene or anisole solutions containing ca 200 ppm of water ($[H_2O]/[Zn] = 0.1$), $[Zn(C_6H_{11})_2]$ decomposes slowly upon heating to yield a black suspension. The black solid which can be isolated from this suspension is immediately oxidized into a white powder upon exposure to air. Transmission electron microscopy (TEM) studies of the black product resulting from the thermolysis of $[Zn(C_6H_{11})_2]$ in anisole (0.27 mol l^{-1}) at 130 °C during 1 h indicate the presence of agglomerated particles with sizes centered near 6 nm and with a narrow size distribution. A typical example of such particles is given in Fig. 1. High resolution transmission electron microscopy (HRTEM) images display fringe patterns as shown in Fig. 2, indicating the crystalline nature of these particles. Surface analysis of the materials by photoemission spectroscopy reveals the presence of both metallic and oxide Auger Zn $2p_{3/2}$ electrons with energies of, respectively 991.2 and 988.1 eV, the XPS Zn $2p_{3/2}$ electrons being observed as a single peak with a binding energy of 1021.8 eV. Brief exposure of the sample to air prior to introduction into the spectrometer and the presence of traces of water in the initial solutions are assumed to be partially at the origin of the presence of zinc oxide at the surface of the particles. The mean size and size distribution is highly dependent upon the reaction time. An important growth of the particles may be observed when the solution is heated for a further 16 h (from 6 to 15 nm) together with a broadening of the size distribution (standard deviation from 0.7 to 2 nm).

Decomposition of $[Zn(C_6H_{11})_2]$ in wet anisole (0.12 mol l^{-1}) containing polyvinylpyrolidone (PVP) with a weight ratio of zinc to PVP fixed at 30%, proceeds slowly at 130 °C to produce, after 3 h, a black colloidal solution of well dispersed nanoparticles as shown in Fig. 3. In contrast to the particles prepared in the absence of PVP, these particles do not appear spherical

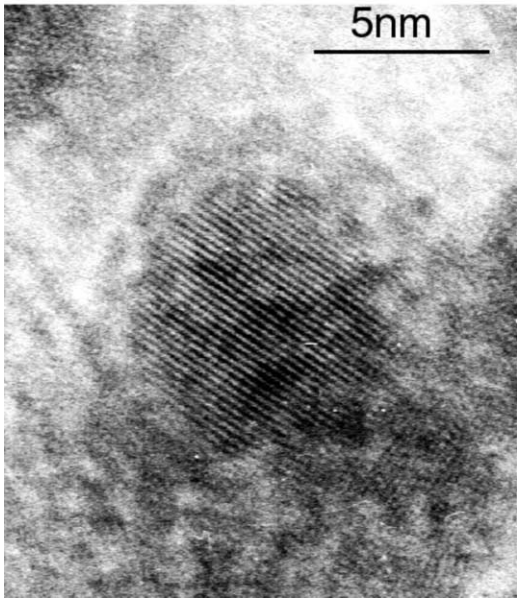

Fig. 2. HRTEM micrograph of zinc nanoparticles evidencing their crystalline structure.

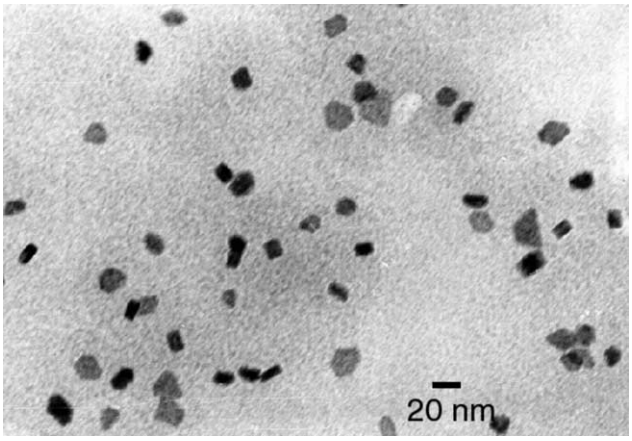

Fig. 3. TEM image showing well-dispersed crystalline small particles of zinc stabilized by PVP.

but display a faceted crystalline aspect with a mean size near 17 nm and a broad size distribution. Fig. 4 shows a typical HRTEM micrograph of these particles and its corresponding numerical diffractogram (Fourier transform). The diffractogram is consistent with the [0001] zone axis pattern of two superimposed hexagonal phases with well-aligned crystalline axes but slightly different parameters. The measurement of the radial distances of the different spots gave the inverse of the $(10\bar{1}0)$ plane spacing in ZnO ($d = 2.815$ Å; inner spots) and in Zn ($d = 2.3036$ Å; outer spots in oblique character in the figure). The sets of spots corresponding to large lattice distances and located close to the center of the pattern originate from the interference of reflections coming from the two different phases and lead to the formation of moiré fringes in the HRTEM image. For instance the horizontal moiré fringes spaced by 2.4 nm correspond to the interference of Zn and ZnO $10\bar{1}0$ reflections. The moiré fringes are only observed in the core of the particle, while the surface region clearly displays the hexagonal lattice of ZnO, the facets being parallel of $(10\bar{1}0)$ type plane. These different features point to Zn particles surrounded by a ZnO crystalline shell, which has grown coherently with the core of the particles. The synthesis and sampling experiments being performed under rigorous anaerobic conditions, the presence of a ZnO surrounding shell is attributed to the water content of the solvents, as previously stated in the case of tin [32–34]. The moisture sensitivity of organozincic compounds is well known and the formation of zinc oxide protected nanoparticles of zerovalent zinc are expected to result from competitive processes involving thermolysis and hydrolysis of the precursor in a similar way to that observed for the growth of [Sn–SnO_x] nanocomposite [34].

The zinc nanoparticles obtained in the absence of PVP were oxidized in air for 3 h at 300 °C and were further oxidized at 600 °C for 3 h. The micrograph displayed in Fig. 5 shows the same type of arrangement of individual particles as in the non-oxidized particles of Fig. 1 as well as no sign of coalescence (average particle size of 8 (0.8) nm). An X-ray diffraction pattern (Fig. 6) indicates the presence of a pure zinc oxide phase adopting the typical hexagonal wurtzite structure.

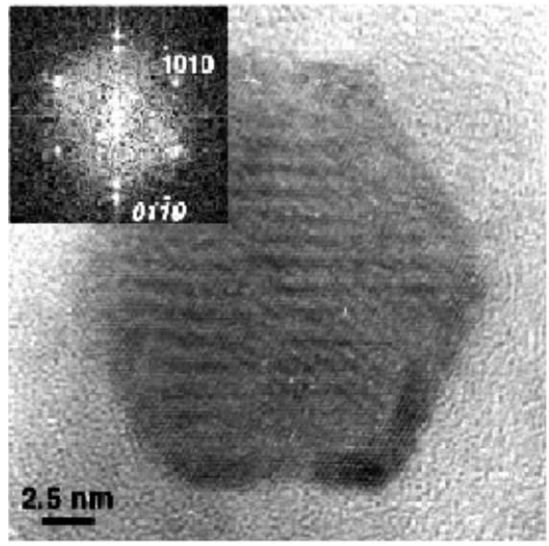

Fig. 4. HRTEM micrograph and corresponding diffractogram (inset) of a Zn nanoparticle stabilized by PVP. Both the image and the numerical spot pattern reveal the presence of a ZnO surface shell surrounding a Zn core. The oblique numbers refer to Zn reflections.

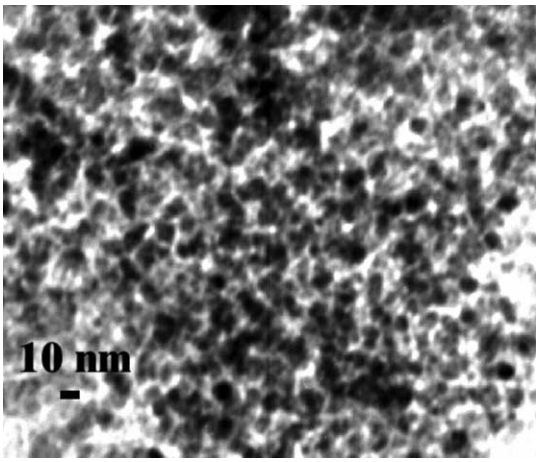

Fig. 5. TEM image of nanoparticles of ZnO prepared by thermal oxidation of Zn nanoparticles.

3. Conclusions

In conclusion, we report in this paper the first synthesis of monodisperse crystalline zinc nanoparticles in mild conditions, using the organometallic complex $[Zn(C_6H_{11})_2]$ as precursor. The particles can be prepared in the presence or in the absence of a polymer. Whatever the synthesis and stabilization modes, the particles display a uniform size and a narrow size distribution. The presence of a zinc oxide layer at the surface of the particles, evidenced by HREM studies, explained that upon thermal treatment in air no coalescence was observed but full oxidation of the particles without changes in their size or morphology. These particles are of interest for applications in microelectronic devices and are presently studied in our laboratory.

4. Experimental

4.1. Materials and reagents

All operations were carried out using standard Shlenk tube or Fischer–Porter bottle techniques under Ar. The preparation of the zinc precursor $[Zn(C_6H_{11})_2]$ follows the route described earlier [36]. It was purified by sublimation, and the resulting highly sensitive white crystals were stored under Ar at -40 °C in a glovebox. Anisole was purchased from Aldrich and its water content was measured by Karl–Fischer coulometric titration, using a Metrohm equipment. Toluene was heated under reflux over sodium in nitrogen atmosphere and distilled just before use.

4.2. Synthesis of zinc nanoparticles

$[Zn(C_6H_{11})_2]$ (1.529 g, 6.6 mmol) in anisole (30 ml) containing traces of water (400 ppm; 0.7 mmol; $[H_2O]/[Zn] = 0.1$) was heated at 130 °C under magnetic stirring in a Fischer–Porter bottle. The initial light yellow solution darkened within 30 min and a black solid

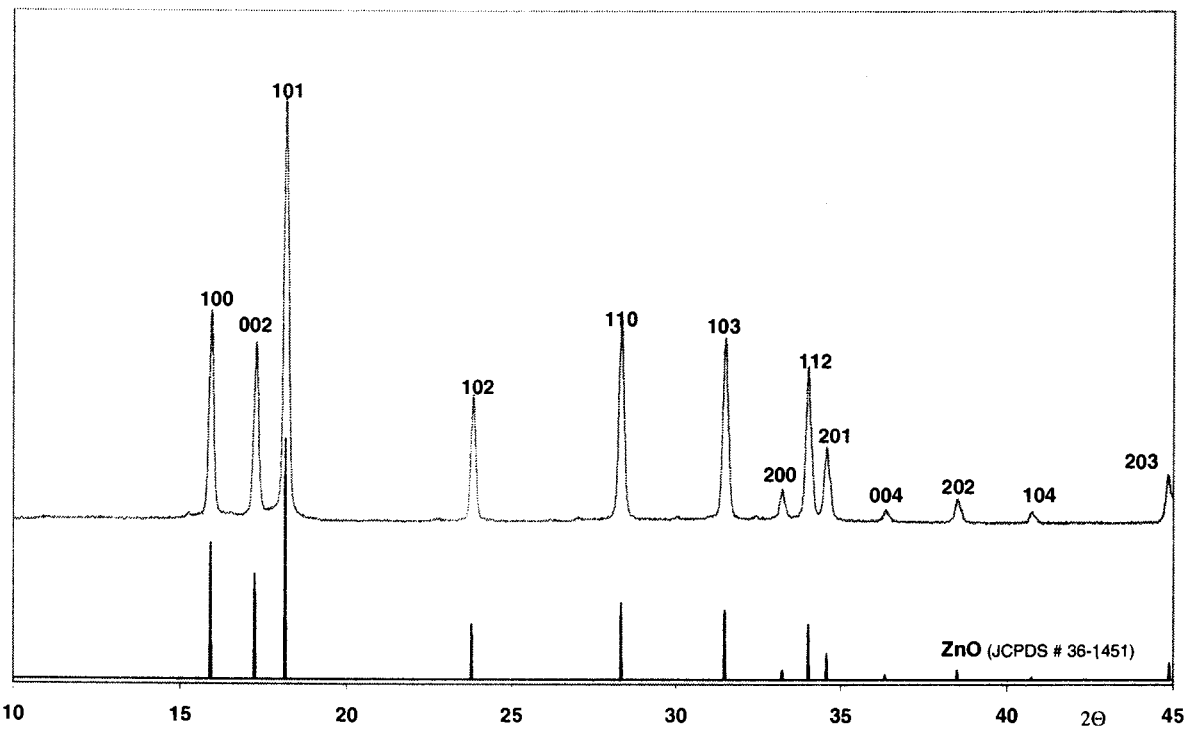

Fig. 6. XRD pattern (Cu–K_α radiation) of nanoparticles of ZnO prepared by thermal oxidation of the nano-Zn particles.

progressively precipitated. After 3 h, the solution was removed by filtration, and the black precipitate was washed with anisole (2×30 ml) and dried under vacuum (135 mg). TEM analysis: Zn nanoparticles, size: 60 (7) Å; yield: 30%.

Thermogravimetric analysis (TGA) of the zinc precursor was obtained on a SETARAM TG-DTA 92 instrument.

In the presence of PVP: $[Zn(C_6H_{11})_2]$ (0.227g; 0.98 mmol) in wet anisole (8 ml; $[H_2O]/[Zn] = 0.2$) was added to PVP (213.5 mg; Zn/PVP = 30/100 mass). The resulting light yellow limpid solution was heated at 130 °C under magnetic stirring in a Fischer–Porter bottle. The solution darkened very slowly and the black limpid solution obtained after 3 h was sampled for TEM and HRTEM experiments.

4.3. Electron microscopy experiments

Samples for TEM and HRTEM studies were prepared in a glove-box by slow evaporation of a drop of suitably diluted colloidal suspensions deposited on holey carbon-covered copper grids. The TEM experiments were performed at the 'Service Commun de Microscopies de l'Université Paul Sabatier' on a JEOL JEM 200CXT-T electron microscope working at 200 kV and a Philips CM12 electron microscope working at 120 kV while the high resolution images were obtained with a JEOL JEM 2010 electron microscope working at 200 kV. The size distribution of the particles was determined from enlarged photographs by measuring a minimum of 200 particles for each sample.

4.4. X-ray photoelectron spectroscopy experiments

Samples for XPS/Auger studies were prepared in a glove-box by slow evaporation of a nanoparticle suspension deposited on a 1 cm^2 silicon support. The spectra were recorded on a VG ESCALAB MKII spectrometer with $Mg-K_\alpha$ radiation.

4.5. X-ray powder diffraction

XRD profile of the oxidized particles deposited on silicon support were obtained with a SEIFERT XRD 3000 TT X-ray diffractometer with $Cu-K_\alpha$ radiation. The data were collected in the grazing incidence configuration.

Acknowledgements

The authors are grateful to V. Collière for assistance with the electron microscopy (Service Commun de Microscopie Electronique de l'Université Paul Sabatier), to G. Chatainier for XPS and Auger spectra to Dr F. Senocq for the measures of X-ray diffraction (ENSI-ACET-INP), and to CNRS for financial support.

References

[1] L. Spanhel, M.A. Anderson, J. Am. Chem. Soc. 113 (1991) 2826.
[2] S. Sakohara, M. Ishida, M.A. Anderson, J. Phys. Chem. Sect. B 102 (1998) 10169.
[3] H. Henglein, Chem. Rev. 89 (1989) 1861.
[4] L. Hozer, Semiconductor ceramics: grain boundary effects, Ellis Horwood and Polish Scientific Publishers PWN, Warsaw, New York, 1994.
[5] X. Wang, S.S. Yee, W.P. Carey, Sens. Actuators Sect. B 24–25 (1995) 454.
[6] C. Xu, J. Tamaki, N. Miura, N. Yamazoe, Sens. Actuators Sect. B 3 (1991) 147.
[7] N. Yamazoe, Sens. Actuators Sect. B 5 (1991) 7.
[8] P.T. Moseley, A.M. Stoneham, D.E. Williams, in: P.T. Moseley, J.O.W. Norris, D.E. Williams (Eds.), Techniques and Mechanisms in Gas Sensing, Adam Hilger, Bristol, Philadelphia and New York, 1991, pp. 108.
[9] D. Kohl, in: G. Sberveglieri (Ed.), Gas Sensors, Principles, Operation and Developments, Kluwer Academic, Dordrecht, Boston, London, 1992, p. 43.
[10] A.V. Chadwick, N.V. Russell, A.R. Whitham, A. Wilson, Sens. Actuators Sect. B 18–19 (1994) 99.
[11] L.F. Dong, Z.L. Cui, Z.K. Zhang, Nanostructured Mater. 8 (1997) 815.
[12] S. Sakohara, L.D. Tickanen, M.A. Anderson, J. Phys. Chem. 96 (1992) 11086.
[13] B.S. Zou, V.V. Volkov, Z.L. Wang, Chem. Mater. 11 (1999) 3037.
[14] S. Fujitsu, H. Toyoda, H. Yanagida, J. Am. Ceram. Soc. 70 (1987) C71.
[15] T.K. Gupta, J. Am. Ceram. Soc. 73 (1990) 1817.
[16] D.F.K. Hennings, R. Hartung, P.J.L. Reijnen, J. Am. Ceram. Soc. 73 (1990) 645.
[17] N. Raghu, T.R.N. Kutty, Appl. Phys. Lett. 60 (1992) 100.
[18] K. Recknagle, Q. Xia, J.N. Chung, C.T. Crowe, H. Hamilton, G.S. Collins, Nanostructured Materials, vol. 4, Elsevier Science Ltd, Amsterdam, New York, 1994, p. 103.
[19] J. Xu, J. Zhang, Y. Du, X. Zhang, Y. Li, Mater. Lett. 29 (1996) 131.
[20] O. Daub, W. Langel, C. Reiner, L. Kienle, Ber. Bunsenges. Phys. Chem. 101 (1997) 1753.
[21] J. Xu, W. Ji, X.B. Wang, H. Shu, Z.X. Shen, S.H. Tang, J. Raman Spectrosc. 29 (1998) 613.
[22] T.G. Cardenas, C.E. Salgado, Polym. Bull. 38 (3) (1997) 279.
[23] T.G. Cardenas, C.R. Oliva, H.H. Carbacho, Bol. Soc. Chil. Quim. 40 (1995) 261.
[24] V.V. Polonski, Y. Yamamoto, M. Kourogi, H. Fukuda, M. Ohtsu, J. Microsc. 194 (1999) 545.
[25] K.-L. Tsai, L. Dye, Chem. Mat. 5 (1993) 540.
[26] M. Respaud, J.M. Broto, H. Rakoto, A.R. Fert, L. Thomas, B. Barbara, M. Verelst, E. Snoeck, P. Lecante, A. Mosset, J. Osuna, T. Ould Ely, C. Amiens, B. Chaudret, Phys. Rev. Sect. B 57 (1998) 2925.
[27] A. Rodriguez, C. Amiens, B. Chaudret, M.J. Casanove, P. Lecante, J.S. Bradley, Chem. Mat. 8 (1996) 1978.
[28] C. Pan, F. Dassenoy, M.-J. Casanove, K. Philippot, C. Amiens, P. Lecante, A. Mosset, B. Chaudret, J. Phys. Chem. Sect. B 103 (1999) 10098.
[29] F. Dassenoy, K. Philippot, T. Ould Ely, C. Amiens, P. Lecante, E. Snoeck, A. Mosset, M.-J. Casanove, B. Chaudret, N. J. Chem. 22 (1998) 703.

[30] O. Vidoni, K. Philippot, C. Amiens, B. Chaudret, O. Balmes, J.-O. Malm, J.-O. Bovin, F. Senocq, J. Casanove, Angew. Chem. Int. Ed. 38 (1999) 3736.
[31] T. Ould Ely, C. Pan, C. Amiens, B. Chaudret, F. Dassenoy, P. Lecante, M.-J. Casanove, A. Mosset, M. Respaud, J.-M. Broto, J. Phys. Chem. Sect. B 104 (2000) 695.
[32] C. Nayral, T. Ould-Ely, A. Maisonnat, B. Chaudret, P. Fau, L. Lescouzeres, A. Peyre-Lavigne, Adv. Mater. 11 (1999) 61.
[33] C. Nayral, E. Viala, V. Collière, P. Fau, F. Senocq, A. Maisonnat, B. Chaudret, Appl. Surf. Sci. 164 (2000) 219.
[34] C. Nayral, E. Viala, P. Fau, F. Senocq, J.-C. Jumas, A. Maisonnat, B. Chaudret, Chem. Eur. J. 6 (2000) 4082.
[35] K. Soulantica, A. Maisonnat, M.-C. Fromen, M.-J. Casanove, P. Lecante, B. Chaudret, Angew. Chem. Int. Ed. 40 (2001) 448.
[36] K.H. Thiele, S. Wilcke, M. Ehrhardt, J. Organomet. Chem. 14 (1968) 13.